Acta Mechanica 188, 39–54 (2007)
DOI 10.1007/s00707-006-0371-2
Printed in The Netherlands

Acta Mechanica

Size-dependent elastic properties of unidirectional nano-composites with interface stresses

T. Chen, Tainan, Taiwan, **G. J. Dvorak**, Troy, New York, and **C. C. Yu**, Tainan, Taiwan

Received February 20, 2006; revised May 3, 2006
Published online: July 20, 2006

Summary. Surfaces and interfaces in solids may behave differently from their bulk counterparts, particularly when the geometry is on the nanoscale. Our objective in this work is to assess the overall behavior of composites containing cylindrical inclusions with surface effects prevailing along the interfaces. In the formulation, we first decompose the loadings into three different deformation modes: the axisymmetric loadings, the transverse shear and the antiplane shear. For each deformation mode, we derive the energy potential incorporating the surface effects. Using a variational approach, we construct the Euler-Lagrange equation together with the natural transition (jump) conditions. The surface effects are represented by an interface of a membrane type, with in-plane moduli different from those of either phase. The overall elastic behavior of the composite is characterized by five constants. Four of them, except the transverse shear modulus, are derived in simple closed forms using an approach of neutral inclusion. For the transverse shear, we derive the value based on the generalized self-consistent method.

1 Introduction

The concept of surface stress dates back to more than one century ago by the celebrated Young-Laplace equation in fluids [1]. Surface tension in fluids is defined as a force per unit length along the perimeter of the interface. The concept of surface stress in solids, first introduced by Gibbs [2], is defined through the change in excess free energy when the interface is deformed at constant referential area. In contrast to fluids, surface stress may not be isotropic, and it may depend on the crystallographic parameters of the solids joined at the interface. Recent atomistic calculations indicate that a solid surface can be either elastically softer or stiffer than their bulk counterparts [3]. The effect of surface stress has recently received substantial attention in the materials physics community. Numerous studies focused on the subjects of thin film stress evolution during deposition (see, for example, Cammarata et al. [4], [5], Freund and Suresh [6] and the references contained therein).

A different application of surface effects is concerned with nanocomposites. The significance of surfaces becomes important in nanoscaled structures due to their high surface-to-volume ratios. The strain energy in these structures can be dramatically influenced by surface effects and subsequently alters their local behavior and macroscopic properties. The objective of this work is to explore the macroscopic behavior of nano-composites incorporating the surface effect. Relevant to this line of research, Sharma et al. [7] derived solutions for the elastic state of eigenstrained spherical inhomogeneities with surface effects using variational approaches. They

found that surface elasticity can significantly change the local fields at nanosized inclusion. Yang [8] derived the effective bulk and shear moduli of composites containing spherical nanosized cavities at dilute concentrations, in which the surface behavior is simply modelled by a constant residual tension. Sharma and Ganti [9] derived closed-form expressions for the Eshelby's tensor for spherical and cylindrical inclusions. Duan et al. [10], [11] derived the interior and exterior field solutions for a spherical inhomogeneity with the interface stress effect subjected to a uniform eigenstrain in the inclusion and/or to a remote uniform stress. In all these studies, apart from the work of Sharma and Ganti [9] which considered the Eshelby tensor to cylindrical inclusions, attention has been limited to spherical inclusions.

Our objective in this work is to assess the overall elastic behavior of composites with aligned cylindrical inclusions with surface effects along the interfaces. We consider that the phase constituents are elastically transversely isotropic and the interfacial property is taken as isotropic. Macroscopically, the overall behavior will be transversely isotropic, characterized by five effective constants for the nanocomposites. For the mechanical properties, we can decompose the loadings into three different deformation modes: the axisymmetric loadings, the transverse shear and the antiplane shear. We first derive the energy potential incorporating the surface effects for each deformation mode. Using the variational approach, one can construct the Euler-Lagrange equation together with the interface jump conditions. The interface conditions are described as a continuity of tangential strain across the interface in conformity with the coherent interface assumption as well as a jump condition in traction. The latter term comes from the natural transition condition in the variational process.

Derivation of local fields and overall properties relies on construction of neutral inclusions, or in the same spirit, on composite cylinder assemblages [12]. The four effective elastic constants are derived in simple closed forms. The remaining transverse shear modulus, based on the generalized self-consistent method, could also be calculated through simple algebra. The analytic expressions for evaluation of overall properties may serve is selecting phase properties and volume fractions that would yield desirable overall moduli.

The plan of the paper is as follows. In Sect. 2, we derive the free energy of the system for three different loading types. By using a variational approach, Euler equations together with the interface conditions are found. The effective mechanical properties are derived in Sect. 3. The axisymmetric moduli and the antiplane shear modulus are derived using an idea of neutral inclusions. For the effective transverse shear modulus, we derive the value using the generalized self-consistent method. Numerical calculations are illustrated in Sect. 4 for field solutions as well as for the effective moduli. Finally, some concluding remarks are made in Sect. 5.

2 Interface conditions with surface stress

Here we are concerned with the boundary of a circular cylinder, in which the interface between the two sides (the inclusion and the matrix) is associated with a deformation dependent interfacial energy $\mathscr{G}$. The fiber composite is modeled here by a representative volume element consisting of aligned circular cylindrical fibers of the same diameter, bonded to the matrix by a coherent interface which has a deformation-dependent surface energy and thus allows for discontinuous radial tractions. The composite cylinder model is adopted for evaluation of local fields in the phases that are used in Sect. 3 in the derivation of overall moduli.

Both fiber and matrix phases are assumed to be transversely isotropic, with the z-axis of symmetry. The phase constitutive relation can be written as

$$\begin{pmatrix} \sigma_r^k \\ \sigma_\theta^k \\ \sigma_z^k \end{pmatrix} = \begin{pmatrix} k+m & k-m & l \\ k-m & k+m & l \\ l & l & n \end{pmatrix}^k \begin{pmatrix} \varepsilon_r^k \\ \varepsilon_\theta^k \\ \varepsilon_z^k \end{pmatrix}, \tag{2.1}$$

$$\sigma_{rz}^k = 2p_k\varepsilon_{rz}^k,\ \sigma_{\theta z}^k = 2p_k\varepsilon_{\theta z}^k,\ \sigma_{r\theta}^k = 2m_k\varepsilon_{r\theta}^k,$$

where the index $k = f, m$ denotes the inclusion and the matrix, respectively, and the coefficients k, l, n, m, p are Hill's moduli [13].

Surface/interface stress can be defined in various ways. A review of these effects was given by Cammarata [17], see also the earlier works of Gibbs [2], Shuttleworth [15] and Herring [16]. The interfacial or surface energy is positive definite. Two independent interface stresses have been reported in the literature: one is associated with coherent interface in which the tangential strains are equal on both sides of the phases, the other allows that different tangential strains may occur at the interface [17]. In the present study we are concerned with the first mode of deformation in which no atomic bonds are broken in the interface plane. Interface stresses can be described as (2×2) symmetric tensors in the tangent plane (strains normal to the surface are excluded). The surface stress tensor, $\sigma_{\alpha\beta}^s$, is related to the deformation dependent surface energy $\mathscr{G}(\varepsilon_{\alpha\beta})$ by [15], [18]

$$\sigma_{\alpha\beta}^s = \frac{\partial \mathscr{G}}{\partial \varepsilon_{\alpha\beta}^s} + \tau_0\delta_{\alpha\beta}, \tag{2.2}$$

where $\varepsilon_{\alpha\beta}^s$ is the (2×2) surface strain tensor, $\delta_{\alpha\beta}$ is the Kronecker delta for surfaces and the constant τ_0 is the residual surface tension. Equation (2.2) can be interpreted as modeling the surface between the fiber and the matrix as an elastic skin, or interfacial thin layer that is stretched over the bulk of two sides. In general those interface properties will be anisotropic which depend on the crystallographic directions. Here in the sequel, the interface is taken as elastically isotropic. The effect of residual tension τ_0 is not considered here. The surface moduli can then be characterized by the surface Lamé constants λ_s and μ_s as [7], [9]

$$\sigma_{\beta\alpha}^s = 2\mu_s\varepsilon_{\beta\alpha}^s + \lambda_s\varepsilon_{\gamma\gamma}^s\delta_{\beta\alpha}. \tag{2.3}$$

Conventional summation rules apply unless otherwise stated. Note that the Greek indices take on values of the interfacial component. For instance, for cylindrical inclusions, $\alpha, \beta = \theta, z$. The surface moduli λ_s, μ_s have the dimensions of N/m which is different from the standard Lamé constants (N/m^2).

2.1 Axisymmetric deformations

We consider a composite cylinder which is composed of a circular fiber with radius a surrounded with a concentric shell of matrix with outer radius b. Suppose that on the outer boundary of the composite cylinder the matrix is subjected to the homogeneous boundary conditions

$$\varepsilon_r|_{r=b} = e, \quad \varepsilon_z = \varepsilon_0. \tag{2.4}$$

The in-plane displacement fields are independent of the circumferential and axial variables, θ and z, and the axial displacement is simply a linear function of z. That is $u_r^k = u_k(r)$, $u_\theta^k = 0$ and $u_z^k = \varepsilon_0 z$. To proceed, the free energy of the composite cylinder under (2.4), in the presence of surface effects, can be written as

$$\Pi = \int_0^{2\pi}\int_0^{a} \Psi_f r dr d\theta + \int_0^{2\pi}\int_a^{b} \Psi_m r dr d\theta + \int_0^{2\pi} \Psi_s a d\theta, \tag{2.5}$$

where the bulk and surface elastic energy densities are functions of r, expressed as

$$\Psi_k\big(r, u_k(r), u_k'(r)\big) = \frac{1}{2}\sigma_{ij}^k \varepsilon_{ij}^k, \Psi_s(u_s) = \int_0^{\varepsilon_{ij}^s} \sigma_{ij}^s d\varepsilon_{ij}^s, \tag{2.6}$$

and the prime denotes derivatives with respect to r. As the displacement fields need to fulfill the prescribed boundary conditions (2.4) (essential boundary conditions), by setting the variation of the free energy to be zero, i.e., $\delta\Pi = 0$, we obtain the Euler-Lagrange equation

$$\frac{d^2u_k}{dr^2} + \frac{1}{r}\frac{du_k}{dr} - \frac{u_k}{r^2} = 0. \tag{2.7}$$

We require that the minimizing (or maximizing) function be continuous at $r = a$ in conformity with the coherent interface assumption, in which all admissible displacements possess the common variation along the interface $\delta u_f\big|_{r\to a} = \delta u_m|_{r\to a} = \delta u_s$. Then we are led to the natural transition condition along the interface

$$\left[\frac{\partial F_f}{\partial u_f'} - \frac{\partial F_m}{\partial u_m'} + (\lambda_s + 2\mu_s)\frac{u_s}{a}\right]_{r\to a} \delta u_s = 0, \tag{2.8}$$

where the functional $F_k = r\Psi_k$. Then, substituting F_k into Eq. (2.8) will give the jump condition on stress. Specifically, the interface conditions are given by

$$u_f(r)\big|_{r=a} = u_m(r)|_{r=a}, \quad \sigma_{rr}^m - \sigma_{rr}^f = \left.\frac{\sigma_{\theta\theta}^s}{r}\right|_{r=a}. \tag{2.9.1,2}$$

The presence of surface stress gives rise to a nonclassical boundary condition, which in combination with the surface stress-strain relations and the equations of classical elasticity form a coupled system of field equations. The governing field (2.7), together with the interface conditions (2.9) and the boundary conditions (2.4), will allow us to determine the field solutions.

2.2 Transverse shear deformation

Next we consider a transverse shear deformation in which the boundary data, $u_x = cx$, $u_y = -cy$, $u_z = 0$, are prescribed on the surface $r = b$. In terms of cylindrical coordinates, these fields correspond to $u_r = cr\cos 2\theta$, $u_\theta = -cr\sin 2\theta$, $u_z = 0$, where the value c is the applied shear strain. The displacement fields of the composite cylinder under the transverse shear can then be written as:

$$u_r^k = U_k(r)\cos 2\theta, \quad u_\theta^k = V_k(r)\sin 2\theta, \quad u_z^k = 0, \tag{2.10}$$

where $U_k(r)$, $V_k(r)$ and $W_k(r)$ are unknown functions of r. The nonvanishing strain components are:

$$\varepsilon_r^k = \frac{dU_k}{dr}\cos 2\theta, \quad 2\varepsilon_{r\theta} = \sin 2\theta\left(\frac{dV_k}{dr} - \frac{V_k}{r} - \frac{2U_k}{r}\right),$$

$$\varepsilon_\theta^k = \frac{\cos 2\theta}{r}(U_k + 2V_k), \quad \varepsilon_\theta^s = \frac{\cos 2\theta}{a}(U_k(a) + 2V_k(a)), \tag{2.11}$$

and the corresponding stresses can be derived accordingly. Again the interface of the inclusion and the matrix is endowed with a deformation dependent interfacial energy $\mathscr{G}$. We first derive the free energy of the composite system Π. In contrast to the axisymmetric loadings, the strain energy density now depends on r as well as on θ. Setting $\delta\Pi = 0$ and allowing that the variations $\delta U_k(r)$ and $\delta V_k(r)$ be arbitrarily varied, the Euler-Lagrange equations,

$$\frac{\partial F_k}{\partial U_k} - \frac{\partial}{\partial r}\left(\frac{\partial F_k}{\partial U_k'}\right) = 0, \quad \frac{\partial F_k}{\partial V_k} - \frac{\partial}{\partial r}\left(\frac{\partial F_k}{\partial V_k'}\right) = 0, \tag{2.12}$$

with

$$F_k\big(r, U_k, U_k', V_k, V_k'\big) = \int_0^{2\pi} r\Psi_k d\theta, \quad F_s = a\int_0^{2\pi} \Psi_s\big(a, u_{(s)}\big)d\theta, \tag{2.13}$$

can be expanded as

$$\begin{aligned} &U_k'' + \frac{U_k'}{r} - \frac{k_k + 5m_k}{k_k + m_k}\frac{U_k}{r^2} + \frac{2k_k}{k_k + m_k}\frac{V_k'}{r} - \frac{2(k_k + 2m_k)}{k_k + m_k}\frac{V_k}{r^2} = 0, \\ &-\frac{2k_k}{m_k}U_k' - 2\frac{k_k + 2m_k}{m_k}\frac{U_k}{r^2} + V_k'' + \frac{V_k'}{r} - \frac{4k_k + 5m_k}{m_k}\frac{V_k}{r^2} = 0. \end{aligned} \tag{2.14}$$

We note that, when the phases are isotropic, the system (2.14) is the same as that of the composite system with perfect bonding interface (without the surface effects) [19]. Note that the system of equations (2.14) can also be derived by substituting (2.10) into the equilibrium equations.

To proceed, we note that the functions U_m and V_m need to comply with the boundary conditions. This gives that $\delta U_m = \delta V_m = 0$ at $r \to b$. In addition, to avoid rigid body translation at $r = 0$ we have set $U_f = V_f = 0$. Also we require that the minimizing functions U and V need to be continuous at $r = a$ for coherent interfaces

$$U_f(a) = U_m(a), \quad V_f(a) = V_m(a). \tag{2.15}$$

The remaining boundary terms of $\delta\Pi$ become

$$\left(\frac{\partial F_f}{\partial U_f'}\delta U_f + \frac{\partial F_f}{\partial V_f'}\delta V_f\right)\Big|_{r\to a} - \left(\frac{\partial F_m}{\partial U_m'}\delta U_m + \frac{\partial F_m}{\partial V_m'}\delta V_m\right)\Big|_{r\to a} + \delta F_s = 0. \tag{2.16}$$

These are exactly the natural transition conditions in the theory of variation ([20], p. 129). Upon substitution of Eqs. (2.13) into (2.16), we find the interfacial jump conditions

$$\hat{\sigma}_{rr}^m(r) - \hat{\sigma}_{rr}^f(r)\big|_{r\to a} = \frac{(\lambda_s + 2\mu_s)(U_s + 2V_s)}{r}\Big|_{r\to a}, \tag{2.17}$$

$$\hat{\sigma}_{r\theta}^m(r) - \hat{\sigma}_{r\theta}^f(r)\Big|_{r\to a} = \frac{2(\lambda_s + 2\mu_s)(U_s + 2V_s)}{r}\Big|_{r\to a}, \tag{2.18}$$

where the hat quantities, independent of θ, are given by

$$\sigma_{rr}^k(r,\theta) = \hat{\sigma}_{rr}^k(r)\frac{\cos 2\theta}{a}, \quad \sigma_{r\theta}^k(r,\theta) = \hat{\sigma}_{r\theta}^k(r)\frac{\sin 2\theta}{a}. \tag{2.19}$$

In the absence of surface residual tension τ_0, the conditions (2.17) and (2.18) can be further simplified to

$$\sigma_{rr}^m(r) - \sigma_{rr}^f(r)\big|_{r\to a} = \frac{\sigma_{\theta\theta}^s}{r}\Big|_{r\to a}, \quad \sigma_{r\theta}^m(r) - \sigma_{r\theta}^f(r)\Big|_{r\to a} = -\frac{1}{r}\frac{\partial\sigma_{\theta\theta}^s}{\partial\theta}\Big|_{r\to a}. \tag{2.20}$$

Note that if we look at the various types of imperfect interfaces proposed by Benveniste and Miloh [21], we can see that Eqs. (2.9) and (2.20) correspond to the membrane type of imperfect interface with a suitable choice of the constant P ([21], Eq. (2.11)). Of course, when setting $\lambda_s = \mu_s = 0$, the mathematical framework will recover the known continuity condition of traction.

2.3 Anti-plane shear deformation

We next consider that the composite cylinder is undergoing an antiplane deformation. At the boundary of the matrix the displacement fields, $u_r = 0$, $u_\theta = 0$, $u_z = \varepsilon^0 r \sin\theta$, are imposed. Corresponding to this deformation, the displacement fields of the composite cylinder can be assumed as:

$$u_r^k = 0, \quad u_\theta^k = 0, \quad u_z^k = W_k(r)\sin\theta. \tag{2.21}$$

The non-zero strains are ε_{rz} and $\varepsilon_{\theta z}$. We can now derive the strain energy density. Note that the functional of the phases can be exactly integrated as

$$F_k = \frac{\pi p_k}{2}\left(\frac{W_k^2}{r} + r\left(W_k'\right)^2\right), \quad F_s = 2a\int_0^{2\pi} \mu_s\left(\varepsilon_{\theta z}^s(a)\right)^2 d\theta. \tag{2.22}$$

By setting the variation of the functional be zero, we find the governing equation

$$\frac{d^2 W_k}{dr^2} + \frac{1}{r}\frac{dW_k}{dr} - \frac{1}{r^2}W_k = 0. \tag{2.23}$$

Further, the function W_m needs to satisfy the boundary condition. This implies that $\delta W_m = 0$ at $r \to b$. In addition, we have set $W_f = 0$ at the origin $r = 0$ to avoid rigid body translation. We further require that $W_f(a) = W_m(a)$ due to coherent interface. Then, the remaining terms of $\delta\Pi$ are the natural transition conditions

$$\left(\frac{\partial F_f}{\partial W_f'}\delta W_f\right)\Big|_{r\to a} - \left(\frac{\partial F_m}{\partial W_m'}\delta W_m\right)\Big|_{r\to a} + 2\int_0^{2\pi}\left[\mu_s \varepsilon_{\theta z}^s(a)\cos\theta\right]\delta W\, d\theta = 0, \tag{2.24}$$

which can be written explicitly as

$$\hat{\sigma}_{rz}^m(r) - \hat{\sigma}_{rz}^f(r)\big|_{r\to a} = \frac{\hat{\sigma}_{\theta z}^s}{r}\Big|_{r\to a}, \tag{2.25}$$

where the hat quantities, depending only on r, are defined as

$$\sigma_{rz}^k(r,\theta) = \hat{\sigma}_{rz}^k(r)\sin\theta, \quad \sigma_{\theta z}^s(r,\theta) = \hat{\sigma}_{\theta z}^s(r)\cos\theta. \tag{2.26}$$

We mention that the interfacial jump conditions in traction, (2.9.2), (2.20) and (2.25), under the three different deformation modes agree exactly with the analysis of the generalized Young-Laplace equations for solids obtained by Povstenko [22]. Here we recapitulate the main results in Appendix A.

3 Effective elastic properties

In this Section we will derive the effective moduli of k^*, l^*, n^* and p^* using the concept of neutral inhomogeneities ([23], Chap. 7). The idea of neutral inhomogeneity is mathematically equivalent to that of constructions of composite cylinder assemblages (CCA) [13]. It is known

that for perfect bonding interfaces (i.e., without surface effect), the effective moduli by the CCA model have the same form as those predicted by the Mori-Tanaka method [24] and lie within variational bounds [25]. For the effective transverse shear m^*, we use the generalized self-consistent model (GSCM) [19] (or called three-phase model) to derive the effective transverse shear modulus.

3.1 Effective axisymmetric moduli k^*, l^*, n^*

We first consider the composite cylinder is under the loading (2.4). The admissible displacement fields, by solving Eq. (2.7), can be written as

$$u_r^f = Ar, \quad u_r^m = Br + \frac{C}{r}, \quad u_z^f = u_z^m = \varepsilon_0 z, \quad u_\theta^f = u_\theta^m = 0, \tag{3.1}$$

where the coefficients A, B, C are constants that need to be determined from the boundary and interface conditions, (2.4) and (2.9). Next we consider a homogeneous cylinder with the same size of the composite cylinder, with the effective moduli being denoted by k^*, l^*, n^*. Under the same boundary condition (2.4), we wish to adjust the values of k^*, l^*, n^* so that the radial stress at $r = b$ and the average axial stress in both configurations are the same. This concept can be interpreted in different ways, termed as the CCA, or as the replacement inhomogeneity. Specifically, these effective moduli can be exactly found as

$$k^* = k_m + c_f \frac{(k_m + m_m)\left[k_f - k_m + \frac{\lambda_s + 2\mu_s}{2a}\right]}{k_f + m_m - c_f(k_f - k_m) + c_m \dfrac{\lambda_s + 2\mu_s}{2a}}, \tag{3.2}$$

$$l^* = l_m + c_f \frac{(k_m + m_m)\left(l_f - l_m + \frac{\lambda_s}{a}\right)}{k_f + m_m - c_f(k_f - k_m) + c_m \dfrac{(\lambda_s + 2\mu_s)}{2a}}, \tag{3.3}$$

$$n^* = c_f n_f + c_m n_m + c_f \frac{2(\lambda_s + 2\mu_s)}{a} - \frac{c_f c_m \left(l_f + \frac{\lambda_s}{a} - l_m\right)^2}{k_f + m_m - c_f(k_f - k_m) + c_m \dfrac{\lambda_s + 2\mu_s}{2a}}. \tag{3.4}$$

When setting $\lambda_s = \mu_s = 0$, it is seen that the formulae for k^*, l^* and n^*, recover the known classical expressions for the perfect bonding situations ([13], Eqs. (3.6), (3.8)).

3.2 Effective antiplane shear modulus p^*

We now derive the effective antiplane shear modulus p^*. The admissible displacement fields, following from the governing equation (2.23), are

$$u_r^f = u_r^m = 0, \quad u_\theta^f = u_\theta^m = 0, \quad u_z^f = Ar\sin\theta, \quad u_z^m = \left(Br + \frac{C}{r}\right)\sin\theta, \tag{3.5}$$

where again the constants A, B and C can be found from the boundary condition and the interface conditions. Next we consider a same-size homogeneous cylinder with the unknown axial shear modulus p^*. Under the same boundary condition, we wish to adjust the value of

p^* so that the shear traction σ_{rz} at $r = b$ will be the same in both configurations. This will give

$$p^* = p_m \frac{(1+c_f)\left(p_f + \frac{\mu_s}{a}\right) + (1-c_f)p_m}{(1-c_f)\left(p_f + \frac{\mu_s}{a}\right) + (1+c_f)p_m}. \tag{3.6}$$

When the interface effect is neglected, the effective antiplane shear modulus again reduced to the classical perfect bonding result for p^* [13].

3.3 Effective transverse shear modulus m^*

For the transverse shear loading, it is not possible to construct a neutral composite cylinder. A commonly adopted procedure to derive the effective transverse shear modulus is through the generalized self-consistent method. For a detailed exposition of this method, one can refer to the work of Christensen and Lo [19]. This model assumes that the inclusion is first surrounded by some matrix material, and then embedded in an effective medium with unknown effective shear modulus. The auxiliary boundary value problem to be solved is that of a composite cylinder with a cylindrical core with a matrix shell embedded in the unknown effective medium (designated by $*$), and subjected at the remote boundary to a tranverse shear boundary condition $u_x|_{r\to\infty} = cx,\ u_y|_{r\to\infty} = -cy,\ u_z = 0$. Note that the boundary condition and the geometric configuration considered in Sect. 2.2 suffices to model the case of the generalized self-consistent method employed here as the radius b can be taken as infinity. Under the deformation, the corresponding solutions to Eqs. (2.14) have the forms

$$\begin{aligned}
u_r^f &= \frac{b}{4m_f}\left(D_1\left(\frac{r}{b}\right) + A_1(\eta_f - 3)\left(\frac{r}{b}\right)^3\right)\cos 2\theta,\\
u_\theta^f &= \frac{b}{4m_f}\left(-D_1\left(\frac{r}{b}\right) + A_1(\eta_f + 3)\left(\frac{r}{b}\right)^3\right)\sin 2\theta,
\end{aligned} \tag{3.7}$$

$$\begin{aligned}
u_r^m &= \frac{b\cos 2\theta}{4m_m}\left(A_2(\eta_m - 3)\left(\frac{r}{b}\right)^3 + D_2\left(\frac{r}{b}\right) + C_2(\eta_m + 1)\left(\frac{b}{r}\right) + B_2\left(\frac{b}{r}\right)^3\right),\\
u_\theta^m &= \frac{b\sin 2\theta}{4m_m}\left(A_2(\eta_m + 3)\left(\frac{r}{b}\right)^3 - D_2\left(\frac{r}{b}\right) - C_2(\eta_m - 1)\left(\frac{b}{r}\right) + B_2\left(\frac{b}{r}\right)^3\right),
\end{aligned} \tag{3.8}$$

$$\begin{aligned}
u_r^* &= \frac{b}{4m^*}\left(2\frac{r}{b} + A_3(\eta^* + 1)\left(\frac{b}{r}\right) + C_3\left(\frac{b}{r}\right)^3\right)\cos 2\theta,\\
u_\theta^* &= \frac{b}{4m^*}\left(-2\frac{r}{b} - A_3(\eta^* - 1)\left(\frac{b}{r}\right) + C_3\left(\frac{b}{r}\right)^3\right)\sin 2\theta,
\end{aligned} \tag{3.9}$$

where

$$\eta^* = 1 + 2\frac{m^*}{k^*}, \quad \eta_m = 1 + 2\frac{m_m}{k_m}, \quad \eta_f = 1 + 2\frac{m_f}{k_f}. \tag{3.10}$$

The eight constants, A_1, D_1, A_2, B_2, C_2, D_2, A_3 and C_3 can be determined from the eight interface conditions:

$$u_r^f\big|_{r=a} = u_r^m\big|_{r=a}, \quad u_r^m\big|_{r=b} = u_r^*\big|_{r=b}, \quad u_\theta^f\Big|_{r=a} = u_\theta^m\big|_{r=a},$$

$$u_\theta^m\big|_{r=b} = u_\theta^*\big|_{r=b}, \quad \sigma_r^m\big|_{r=b} = \sigma_r^*\big|_{r=b}, \quad \sigma_{r\theta}^m\big|_{r=b} = \sigma_{r\theta}^*\big|_{r=b}, \tag{3.11}$$

$$\int_0^{2\pi} \sigma_r^m(a,\theta)\cos 2\theta\, d\theta - \int_0^{2\pi} \sigma_r^f(a,\theta)\cos 2\theta\, d\theta = \frac{1}{a}\int_0^{2\pi} \sigma_\theta^s \cos 2\theta\, d\theta\Big|_{r=a},$$

$$\int_0^{2\pi} \sigma_{r\theta}^m(a,\theta)\sin 2\theta\, d\theta - \int_0^{2\pi} \sigma_{r\theta}^f(a,\theta)\sin 2\theta\, d\theta = \frac{2}{a}\int_0^{2\pi} \sigma_\theta^s \cos 2\theta\, d\theta\Big|_{r=a}. \tag{3.12}$$

Note that these field quantities depend on the unknown effective shear modulus m^* as well as the effective plane strain bulk modulus k^*. Next we consider a homogeneous comparison medium with the effective shear modulus m^*, which is subjected to the same boundary condition. This will give the referenced field

$$u_r^0 = \frac{r}{2m^*}\cos 2\theta, \quad u_\theta^0 = -\frac{r}{2m^*}\sin 2\theta, \quad \sigma_r^0 = \cos 2\theta, \quad \sigma_{r\theta}^0 = -\sin 2\theta. \tag{3.13}$$

To proceed, we employ Eshelby's formula [26] for the strain energy of the system

$$\int_0^{2\pi} \left(\sigma_r^* u_r^0 + \sigma_{r\theta}^* u_\theta^0 - \sigma_r^0 u_r^* - \sigma_{r\theta}^0 u_\theta^*\right) b\, d\theta = 0. \tag{3.14}$$

Upon a substitution of the field quantities into the identity (3.14), it can be proven analytically through the software Mathematica that

$$A_3 = 0. \tag{3.15}$$

As remarked by Christensen and Lo [27], a more direct way to resolve the solution of m^* is to set Eq. (3.15) into (3.9) at the outset. Carrying through the derivations (3.11) and (3.12), this will give an algebraic system of eight equations with eight unknowns, A_1, D_1, A_2, B_2, C_2, D_2, C_3, m^*. For completeness, the system of equations is recorded in Appendix B. The solution for m^* can be written in terms of a quadratic equation for m^*. In the absence of the surface effects, we have checked analytically that our system of equations exactly agrees with that of Christensen and Lo [19].

4 Numerical results

In numerical illustrations, we first examine the effect of surface stress on the field solutions. We consider a cylindrical cavity in an unbounded isotropic matrix (by letting $b \to \infty$) subjected to a remote transverse hydrostatic tension $\sigma_r^m\big|_{r\to\infty} = \sigma^0$, with an axial constraint $\varepsilon_z = 0$. Based on the preceding derivations, the stress concentration factor (SCF) along the boundary of the cylindrical cavity can be written as

$$SCF = \frac{\sigma_\theta^m}{\sigma^0}\Big|_{r\to a} = \frac{2 + \dfrac{\lambda_s + 2\mu_s}{2a}\left(\dfrac{1}{m_m} - \dfrac{1}{k_m}\right)}{1 + \dfrac{\lambda_s + 2\mu_s}{2a}\dfrac{1}{m_m}}. \tag{4.1}$$

The same geometric configuration subjected to a remote transverse shear $\sigma_x^m|_{r\to\infty} = -\sigma_y^m\Big|_{r\to\infty} = \sigma^0$ is also considered. The hoop stress around the cavity surface can be found as

$$SCF = \frac{\sigma_\theta^m}{\sigma^0}\Big|_{r\to a} = -\frac{4 + \dfrac{\lambda_s + 2\mu_s}{a}\left(\dfrac{1}{m_m} - \dfrac{1}{k_m}\right)}{1 + \dfrac{\lambda_s + 2\mu_s}{2a}\left(\dfrac{2}{m_m} + \dfrac{1}{k_m}\right)}\cos 2\theta. \tag{4.2}$$

Note that when the surface effect is neglected, or the radius of the cylindrical cavity a is relatively large, Eq. (4.1) gives a concentration factor of 2 and Eq. (4.2) gives a concentration factor of 4. Both of which agree with the classical elasticity solutions [28]. To make numerical illustrations, we consider solids containing cylindrical cavities. The material properties of the matrix are recorded from [11] for aluminium ($K_f = 75.2$ GPa, $\nu_f = 0.3$). Note that K is the isotropic bulk modulus and μ is the shear modulus, which are related to Hill's moduli by $k = K + \mu/3$, $\mu = p = m$. The free surface properties were extracted from the existing literature which were calculated based on the molecular dynamics simulations [29]. The surface properties generally vary with different crystallographic orientations. Here we adopted two different sets of surface properties corresponding to the crystallographic directions [100] and [111] of Al. Two sets of the parameters are: surface A, $\lambda_s = 3.48912$ N/m, $\mu_s = -6.2178$ N/m for [100]; surface B, $\lambda_s = 6.842$ N/m, $\mu_s = -0.3755$ N/m for [111]. We shall use surface C to represent the results for the classical solution without interface stress. In Fig. 1, we plotted the stress concentration factor (4.1) under the transverse hydrostatic loading. It is seen that surface A tends to increase the stress concentration as the radius of the cavity becomes smaller. By contrast, surface B reverses the trend. The same calculations for the maximum stress concentration are also made for the transverse shear (Fig. 2). But the factor does increase (decrease) rapidly compared to that of Fig. 1. The classical solution (without surface effects) corresponds to $\lambda_s = \mu_s = 0$, and is thus independent of cavity size.

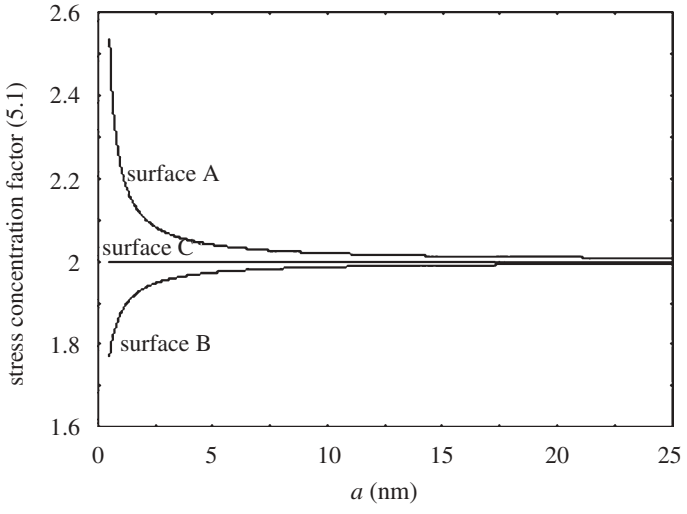

Fig. 1. The stress concentration factor (5.1) of a cylindrical cavity in an unbounded matrix under a hydrostatic transverse loading versus the radius of the cavity. The curve A is calculated based on the surface property of Al [100], curve B uses the surface moduli of Al [111] and the curve C denotes the classical elasticity solution

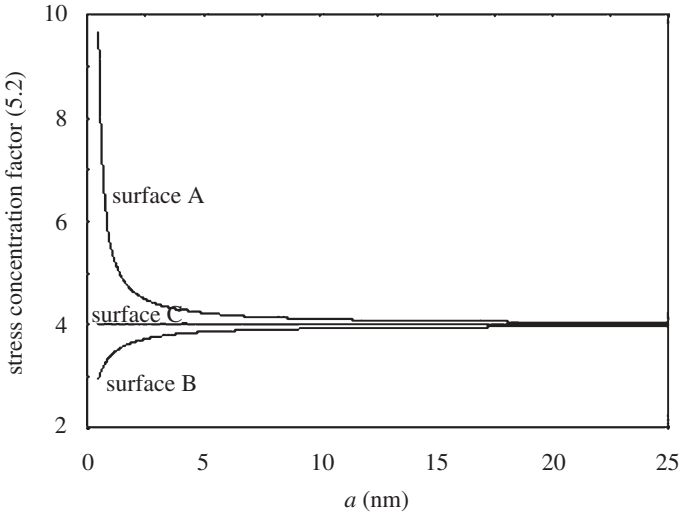

Fig. 2. Same as Fig. 1, but for the transverse shear loading versus the radius of cavity. The stress concentration factor is given in Eq. (5.2)

For the effective moduli, we present k^*/k_C and m^*/m_C, where the subscript C represents the classical results without surface effects. From the formulae (3.2)–(3.4) and (3.6), they suggest that the surface effect becomes important only when the value $(\lambda_s + 2\mu_s)/(2a)$ is in the order of k_f under axisymmetric loadings, and $2\mu_s/a$ is in the order of p_f under antiplane deformation. From the previous surface data (surfaces A and B), it is seen that k_f is around the order of $10 \sim 100$ GPa and λ_s and μ_s are in the order of N/m. From preliminary dimensional analysis, the surface effect will become important when the radius of the fibers, a, is in the order of nanoscale or smaller (10^{-9}m). This observation can also be found from the detailed numerical calculations. In Fig. 3 plots of the value of k^*/k_C versus the cavity radius a (nm) for the volume fraction $c_f = 0.3$ are shown. The surface effect on the effective bulk modulus becomes negligible

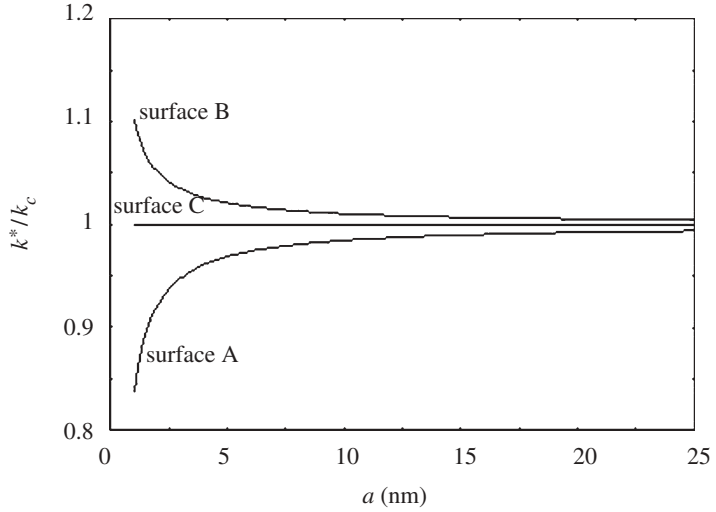

Fig. 3. The value of k^*/k_C versus the radius of the cylindrical cavity a (nm) for the volume fraction $c_f = 0.3$

when the radius of the cavity is larger than 25 nm. A similar plot (Fig. 4) is illustrated for the variations of m^*/m_C versus the cavity radius a. All indicate that when the size of the cavity becomes small, the surface effects become significant. In Figs. 5 and 6, we vary the volume fraction of the cylindrical cavities to assess its influence on the effective quantities. Two different radii of the cavity are selected as $a = 5$ nm and $a = 20$ nm. For a given radius, we plot the effective modulus versus the volume fracion. When the radius size is small, the changing rate becomes more pronounced. These numerical illustrations indicate that the surface effect is particularly significant for smaller sizes of inclusions.

5 Concluding remarks

Surface stress effects with interface stresses can be characterized by a continuity of displacements together with a jump in traction. Mathematically this corresponds to a membrane type of imperfect interface [30]. Although the interface condition can in principle be formulated via an introduction of a very thin and stiff interphase layer between the fiber and the matrix, to deduce the present results from the existing solutions for composites with coated fiber reinforcements would generally require some complicated asymptotic analyses [21], which pose some mathematical difficulties in practice. We demonstrate that this nonclassical interface condition also permits constructions of neutral inclusions. Simple, explicit formulae for four out of the five effective elastic constants have been derived. The remaining transverse shear modulus also permits simple calculations through elementary algebra. The present study may find potential applications in technologically interesting systems, such as nanotube-based composites. The analytic expressions of these properties provide a general guideline for the evaluation of nano-composite systems and thereby to be used to develop criteria for choosing the base combination of different constituent materials to achieve specific purposes.

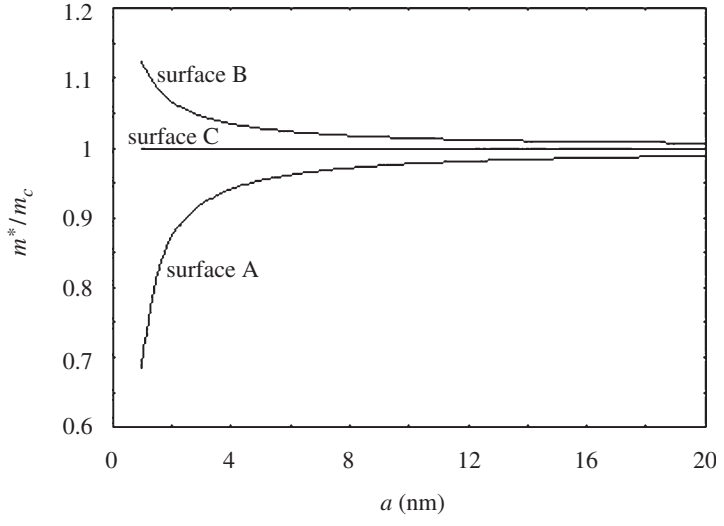

Fig. 4. The value of m^*/m_C versus the radius of the cylindrical cavity a (nm) for the volume fraction $c_f = 0.3$

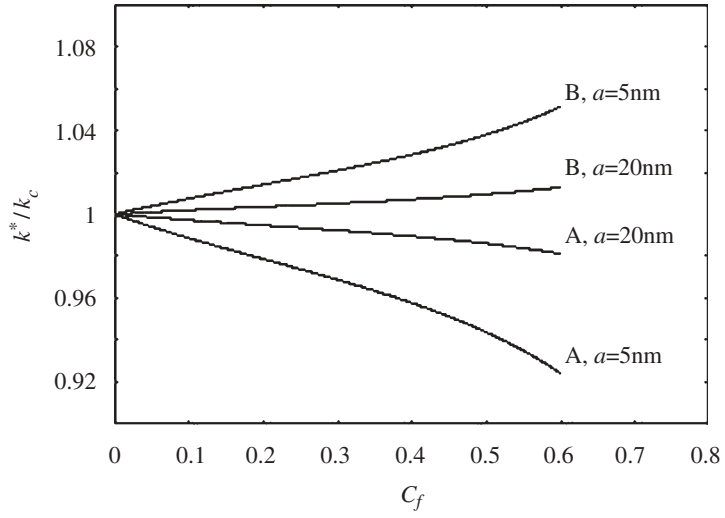

Fig. 5. The value of k^*/k_C versus the volume fraction c_f of the cylindrical cavity for $a = 5$ nm and $a = 20$ nm

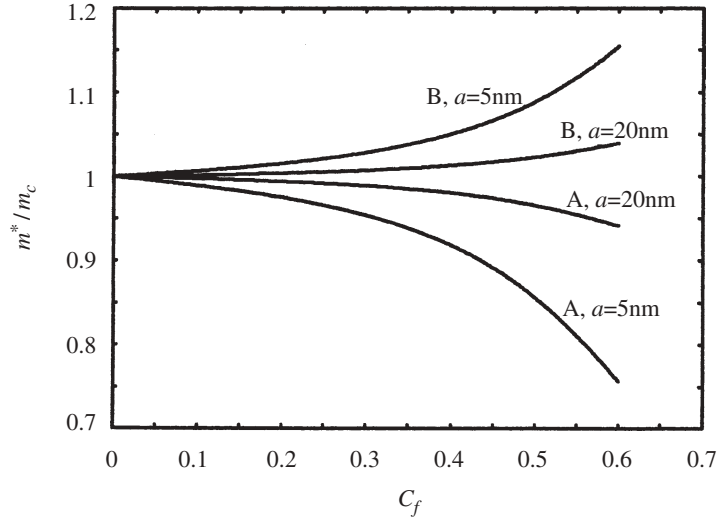

Fig. 6. The value of m^*/m_C versus the volume fraction c_f of the cylindrical cavity for $a = 5$ nm and $a = 20$ nm

Appendix A

Here we record the equilibrium equations of the generalized Young-Laplace equation for solids [22]. The following results are extracted from Duan et al. [10]. The equilibrium equations of the interface can be obtained as

$$\left(\boldsymbol{\sigma}^m - \boldsymbol{\sigma}^f\right) \cdot \mathbf{n} = -\mathbf{V}_S \cdot \boldsymbol{\sigma}^s, \tag{A.1}$$

where $\mathbf{n}$ is the unit normal vector to the interface Γ, and $\nabla_S \cdot \boldsymbol{\sigma}^s$ denotes the surface divergence of $\boldsymbol{\sigma}^s$ at the interface Γ. For a curved interface Γ with two orthogonal unit base vectors $\mathbf{e}_1$ and $\mathbf{e}_2$ in the tangent plane, $\nabla_S \cdot \boldsymbol{\sigma}^s$ is expressed by

$$\nabla_S \cdot \boldsymbol{\sigma}^s = -\left(\frac{\sigma^s_{11}}{R_1}+\frac{\sigma^s_{22}}{R_2}\right)\mathbf{n}+\frac{\mathbf{e}_1}{h_1h_2}\left[\frac{\partial\left(h_2\sigma^s_{11}\right)}{\partial\alpha_1}+\frac{\partial\left(h_1\sigma^s_{21}\right)}{\partial\alpha_2}+\frac{\partial h_1}{\partial\alpha_2}\sigma^s_{12}-\frac{\partial h_2}{\partial\alpha_1}\sigma^s_{22}\right]$$

$$+\frac{\mathbf{e_2}}{h_1h_2}\left[\frac{\partial\left(h_2\sigma^s_{12}\right)}{\partial\alpha_1}+\frac{\partial\left(h_1\sigma^s_{22}\right)}{\partial\alpha_2}-\frac{\partial h_1}{\partial\alpha_2}\sigma^s_{11}+\frac{\partial h_2}{\partial\alpha_1}\sigma^s_{21}\right], \tag{A.2}$$

where α_1 and α_2 denote the two parameters determining the interface such that $\alpha_1 =$ const. and $\alpha_2 =$const. give two sets of a mutually orthogonal curve on Γ, and h_1 and h_2 are the corresponding metric coefficients. R_1 and R_2 are the radii of the principal curvature. For cylindrical inclusions, we can set $\mathbf{e}_1 = \mathbf{e}_\theta$ and $\mathbf{e}_2 = \mathbf{e}_z$, also, $h_1 = r$ and $h_2 = 1$. It can be verified that our interfacial jump conditions in traction are reconstructed.

Appendix B

We outline the system of algebraic equations for the solution of effective shear modulus m^* through the generalized self-consistent method. The system of equations is:

$$\frac{m_m}{m_f}\left[A_1\left(\eta_f-3\right)c_f+D_1\right]=\left[A_2(\eta_m-3)c_f+D_2+C_2(\eta_m+1)c_f^{-1}+B_2c_f^{-2}\right],$$

$$\frac{m_m}{m_f}\left[A_1\left(\eta_f+3\right)c_f-D_1\right]=\left[A_2(\eta_m+3)c_f-D_2-C_2(\eta_m-1)c_f^{-1}+B_2c_f^{-2}\right], \tag{B.1}$$

$$\frac{\eta_m-3}{m_m}A_2+\frac{1}{m_m}D_2+\frac{\eta_m+1}{m_m}C_2+\frac{1}{m_m}B_2=\frac{2}{m^*}+\frac{C_3}{m^*},$$

$$\frac{\eta_m+3}{m_m}A_2-\frac{1}{m_m}D_2-\frac{\eta_m-1}{m_m}C_2+\frac{1}{m_m}B_2=\frac{-2}{m^*}+\frac{C_3}{m^*}, \tag{B.2}$$

$$D_2-4C_2-3B_2+3C_3=2,$$

$$-6A_2+D_2+2C_2+3B_2-3C_3=2, \tag{B.3}$$

$$-3c_f(\eta_m+1)\left(\frac{\lambda_s+2\mu_s}{am_m}\right)A_2+\left(2+\frac{\lambda_s+2\mu_s}{am_m}\right)D_2-2D_1$$

$$+c_f^{-1}\left(-8+(\eta_m-3)\frac{\lambda_s+2\mu_s}{am_m}\right)C_2-3c_f^{-2}\left(2+\frac{\lambda_s+2\mu_s}{am_m}\right)B_2=0, \tag{B.4}$$

$$-6c_fA_1+D_1+c_f\left(6-3(\eta_m+1)\frac{\lambda_s+2\mu_s}{am_m}\right)A_2+\left(-1+\frac{\lambda_s+2\mu_s}{am_m}\right)D_2$$

$$+c_f^{-1}\left(-2+(\eta_m-3)\frac{\lambda_s+2\mu_s}{am_m}\right)C_2-3c_f^{-2}\left(1+\frac{\lambda_s+2\mu_s}{am_m}\right)B_2=0. \tag{B.5}$$

Acknowledgement

This work was initiated while T. Chen was on a summer visit to RPI. GJD and TC were supported by the grant CMS-0409476 from the National Science Foundation. Financial supports to TC were also provided by the U.S. Army Asian Research Office, through an Invitational Travel Order, W2621505IT5045, and from the National Science Council, Taiwan, under contract NSC 93-2211-E006-005.

References

[1] Finn, R.: Equilibrium capillary surfaces. New York: Springer 1986.
[2] Gibbs, J. W.: The collected works of J. W. Gibbs, Vol. 1. p. 315. New York: Longmans 1928.
[3] Zhou, L. G., Huang, H. C.: Are surfaces elastically softer or stiffer? Appl. Phys. Lett. **84**, 1940–1942 (2004).
[4] Cammarata, R. C., Sieradzki, K., Spaepen, F.: Simple model for interface stresses with application to misfit dislocation generation in epitaxial thin films. J. Appl. Phys. **87**, 1227–1234 (2000).
[5] Cammarata, R. C., Trimble, T. M., Srolovitz, D. J.: Surface stress model for instrinsic stresses in thin films. J. Mater. Res. **15**, 2468–2474 (2000).
[6] Freund, L. B., Suresh, S.: Thin film materials: stress, defect formation and surface evolution. Cambridge: Camb. Univ. Press 2003.
[7] Sharma, P., Ganti, S., Bhate, N.: Effect of surfaces on the size-dependent elastic state of nano-inhomogeneities. Appl. Phys. Lett. **82**, 535–537 (2003).
[8] Yang, F. Q.: Size-dependent effective modulus of elastic composite materials: spherical nanocavities at dilute concentrations. J. Appl. Phys. **95**, 3516–3520 (2004).
[9] Sharma, P., Ganti, S.: Size-dependent Eshelby's tensor for embedded nano-inclusions incorporating surface/interface energies. J. Appl. Mech. **71**, 663–671 (2004).
[10] Duan, H. L., Wang, J., Huang, Z. P., Karihaloo, B. L.: Eshelby formalism for nano-inhomogeneities. Proc. R. Soc. Lond. A. **461**, 3335–3353 (2005).
[11] Duan, H. L., Wang, J., Huang, Z. P., Karihaloo, B. L.: Size-dependent effective elastic constants of solids containing nano-inhomogeneities with interface stress. J. Mech. Phys. Solids **53**, 1574–1596 (2005).
[12] Hashin, Z., Rosen, B. W.: The elastic moduli of fiber-reinforced materials. J. Appl. Mech. **31**, 223–232 (1964).
[13] Hill, R.: Theory of mechanical properties of fibre-strengthened materials. I. Elastic behavior. J. Mech. Phys. Solids **12**, 199–212 (1964).
[14] Cammarata, R. C.: Surface and interface stress effects in thin films. Prog. Surf. Sci. **46**, 1–38 (1994).
[15] Shuttleworth, R.: The surface tension of solids. Proc. Phys. Soc. A. **63**, 444–457 (1950).
[16] Herring, C.: The physics of powder metallurgy (Kingston, W. E., ed.), pp.143–179. New York: McGraw-Hill 1951.
[17] Brooks, H.: Metal surface, pp. 30–31. Ohio: American Society for Metals 1952.
[18] Nix, W. D., Gao, H.: An atomistic interpretation of interface stress. Scr. Mater. **39**, 1653–1661 (1998).
[19] Christensen, R. M., Lo, K. H.: Solutions for effective shear properties in three phase sphere and cylinder models. J. Mech. Phys. Solids **27**, 315–330 (1979).
[20] Hildebrand, F. B.: Methods of applied mathematics. Englewood Cliffs: Prentice-Hall 1965.
[21] Benveniste, Y., Miloh, T.: Imperfect soft and stiff interfaces in two-dimensional elasticity. Mech. Mater. **33**, 309–323 (2001).
[22] Povstenko, Y. Z.: Theoretical investigation of phenomena caused by heterogeneous surface tension in solids. J. Mech. Phys. Solids **41**, 1499–1514 (1993).
[23] Milton, G. W.: The theory of composites. Cambridge: Cambridge University Press 2002.
[24] Chen, T., Dvorak, G. J., Benveniste, Y.: Mori-Tanaka estimates of the overall elastic moduli of certain composite materials. J. Appl. Mech. **59**, 539–546 (1992).
[25] Weng, G. J.: The theoretical connection between Mori-Tanaka's theory and the Hashin-Shtrikman-Walpole bounds. Int. J. Engng. Sci. **28**, 1111–1120 (1990).

[26] Eshelby, J. D.: Elastic inclusions and inhomogeneities. In: Progress in solid mechanics 2 (Sneddon, I. N., Hill, R., eds.), pp. 89–140. Amsterdam: North Holland 1961.
[27] Christensen, R. M., Lo, K. H.: Erratum to Christensen and Lo (1979) [19]. J. Mech. Phys. Solids **34**, 639 (1986).
[28] Timoshenko, S. P., Goodier, J. N.: Theory of elasticity. New York: McGraw-Hill 1970.
[29] Miller, R. E., Shenoy, V. B.: Size-dependent elastic properties of nanosized structural elements. Nanotechnology **11**, 139–147 (2000).
[30] Benveniste, Y.: A general interface model for a three-dimensional curved thin anisotropic interphase between two anisotropic media. J. Mech. Phys. Solids **54**, 708–734 (2006).

Authors' addresses: T. Chen and C. C. Yu, Department of Civil Engineering, National Cheng Kung University, Tainan 70101, Taiwan (E-mail: tchen@mail.ncku.edu.tw); G. J. Dvorak, Department of Mechanical, Aerospace & Nuclear Engineering, Rensselaer Polytechnic Institute, Troy, NY 12180–3590, U.S.A.